Long-period comets as a tracer of the Oort cloud structure

Marc Fouchard[1] · Vacheslav Emel'yanenko[2] · Arika Higuchi[3]

Abstract

A previous study showed that a fingerprint of the initial shape of synthetic Oort clouds was detectable in the flux of "new" long-period comets. The present study aims to explain in detail how such a fingerprint is propagated by different classes of observable comets to improve the detection of fingerprints. It appears that three main long-term behaviors of observable comets are involved in this propagation: (1) comets that remain frozen during the entire time span and become observable only because of an increase in their orbital energy at the very end of their propagation; (2) comets whose perihelion distance performs an almost complete galactic cycle, while their galactic longitude of the ascending node and cosine of the galactic inclination remain almost constant; (3) comets whose perihelion distance and cosine of the galactic inclination perform a full galactic cycle, while their galactic longitude of the ascending node performs a half a cycle. This investigation allowed us to define four different zones for the previous perihelion distance, in which one or two of the above long-term behaviors dominate. Considering the distribution of the cosine of the ecliptic inclination and the galactic longitude of the ascending node at the previous perihelion distance, for the different zones, several fingerprints of the initial disk shape were highlighted. Such fingerprints appeared to be quite robust since they were still present considering the reconstructed orbital elements, i.e., the elements obtained from the original orbit after a backward propagation over one orbital period considering only the galactic tides.

Keywords Comets · Oort cloud · Solar System formation

This article is part of the topical collection on Trans-Neptunian Objects
Guest Editors: David Nesvorny and Alessandra Celletti.

✉ Marc Fouchard
   marc.fouchard@obspm.fr

   Vacheslav Emel'yanenko
   vvemel@inasan.ru

   Arika Higuchi
   higuchi.arika@nao.ac.jp

1   Observatoire de Lille, 1 Impasse de l'Observatoire, 50000 Lille, France

2   Institute of Astronomy, Russian Academy of Sciences, Pyatnitskaya Str. 48, Moscow, Russia 119017

3   National Astronomical Observatory of Japan, 2-21-1 Osawa, Mitaka, Tokyo 181-8588, Japan

1 Introduction

The Oort cloud is the furthest structure of the Solar System with an external frontier extending to approximately 0.5 pc. Clearly, direct observations of such a structure are difficult to execute. Our only observable link to the Oort cloud is the flux of long-period comets that reach the inner part of the planetary region of the Solar System. This flux is precisely what led Jan Oort (Oort 1950) to his hypothesis of the existence of the cloud. In particular, it was the accumulation toward zero of the original orbital energy—i.e., the barycentric orbital energy well outside the planetary region before perihelion—of the known long-period comets that helped Jan Oort in making his hypothesis. This accumulation was called the Oort peak.

The reasoning of Oort was that the planetary scattering experienced by these comets made it very unlikely that their orbital energy remained in the Oort peak after the perihelion passage inside the inner part of the planetary system. In other words, in such a case, these comets would be ejected from the Solar System or placed on much smaller orbits, and the observable Oort peak would not persist. From these observations, Oort deduced that the comets in the Oort peak were new, and the Solar System should be surrounded by a cloud of comets between 10000 and 100000 au. Passing stars should thermalize the cloud, i.e., the cloud would become isotropic, and the stars would be responsible for the injection of comets into the observable region.

Owing to the hypothesis of Oort, research has been devoted to the production of the long-period comet flux. Initially, only passing stars were considered; then, galactic tides were thought to be dominant, such that passing stars were almost disregarded. However, in Rickman et al. (2008), it was shown that a synergy is at work between the passing stars and galactic tides.

All these investigations were, in some sense, related to the problem of the mass of the Oort cloud. In Brasser and Morbidelli (2013), the flux of long-period comets, relative to that of Jupiter-family comets, is larger than expected from dynamical models of their source: the Oort cloud and scattered disk. However, these authors assumed a very large value for the physical lifetime of Jupiter-family comets. When the more appropriate value was taken in Vokrouhlický et al. (2019), this discrepancy was reduced substantially. It was shown in Emel'yanenko et al. (2013) that the number of Oort cloud comets corresponding to the observed flux of long-period comets is consistent with that of scattered disk objects corresponding to the flux of Jupiter-family comets.

Regarding the structure of the Oort cloud itself, most of our knowledge originates from numerical simulations from which hypotheses are made concerning the formation process of the Oort cloud. According to Jan Oort, the Oort cloud was isotropic as a consequence of a formation process involving stellar encounters. Later, Hills (1981) developed a model of the flat inner core of the Oort cloud.

In Duncan et al. (1987), the model of the formation from planetary scattering was constructed. They concluded that the Oort cloud should have an inner edge at approximately 3000 au, beyond which the cloud is isotropic. Dones et al. (2004) improved this simulation showing that the Oort cloud should be composed of an inner flat part along the ecliptic plane and an outer part that could be considered as isotropic. The threshold was set at approximately 5000 au.

More recent simulations showed that starting from a flat disk, after 4 Gyr the Oort cloud is isotropic only in the more distant region. It is stressed in Emel'yanenko et al. (2013) that at semimajor axis $a < 6000$ au, the Oort cloud still assumes a strongly flattened structure; however, by $a > 8000$ au, external perturbations have transformed it to be reasonably isotropic.

Fouchard et al. (2017, 2018) found that the Oort cloud is isotropic beyond 10000 au, and the innermost part that is still close to the ecliptic is found at less than approximately 2500 au (for the semimajor axis).

An alternative scenario for the formation of the Oort cloud is that the cloud was formed by stellar encounters when the Sun was still in the cluster where it was born. Regarding the original idea of Oort, such processes produce an Oort cloud for which dispersion with respect to the ecliptic occurs for a semimajor axis, ranging from a few hundred to a few thousand astronomical units, according to the embedded cluster density (Kaib and Quinn 2008; Brasser et al. 2006).

It is clear that since Oort, very little advancement has resulted from the use of observable data in gaining knowledge regarding the Oort cloud structure and, hence, its formation process.

In Fouchard et al. (2018), considering two extreme proto-Oort clouds, one fully isotropic and the second aligned on the ecliptic, the distributions of the original orbital elements of the long-period comets were observed to be very similar, at least from a qualitative perspective. However, it was also observed that a memory of the initial shape of the Oort cloud persists throughout the propagation of the comets. We found that the memory is seen in the distribution of the orbital elements at the perihelion passage preceding that in which the comets are considered to be observable.

The present paper aims to illustrate in detail how observable "new" long-period comets can be used to detect the presence of a disk of objects up to a few thousand astronomical units and how such a fingerprint can be related to the initial shape of the Oort cloud.

The main aspects of the dynamics and formation of the Oort cloud are briefly presented in Sect. 2. Our simulations and the detailed analysis of the flux of observable comets are discussed in Sect. 3. Finally, the conclusions are provided in Sect. 4.

2 The Oort cloud

2.1 Dynamics

For Jan Oort, the comets in the Oort cloud could become observable under the action of passing stars. It was also this idea that led Öpik (1932) to propose the existence of a cloud of comets around the Solar System. However, Öpik did not consider that the cloud could become consequently the origin of long-period comets under the action of passing stars.

Then, in the 1980s, galactic tides came to be considered the main mechanism for transporting comets from the Oort cloud to the inner part of the planetary system. Because observations showed evidence of the role played by the galactic tide (Delsemme 1987), the role of passing stars was downplayed. The role of stars was then reduced to the production of cometary showers caused by a very close encounter of a star with the Sun. During such an event, the star would then be able to inject comets to near-Earth space from the inner part of the Oort cloud, i.e., comets with semimajor axis less than 10000–20000 au from the Sun.

Wiegert and Tremaine (1999) performed the first detailed investigation on the flux of long-period comets coming from the Oort cloud, considering planetary scattering and galactic tides, i.e., neglecting passing stars. The main scope of the paper was to tackle the fading problem of comets, i.e., the lack of "old" long-period comets. The problem is characterized by a dearth of long-period comets outside of the so-called Oort peak (i.e., long-period comets with smaller semimajor axes) compared with "new" comets, that is, comets inside the Oort peak. They

managed to propose a fading law similar to that of Whipple (1962), successfully matching the observed result. Their finding regarding this fading law remains the most accurate until now (Vokrouhlický et al. 2019).

However, Rickman et al. (2008) have shown that passing stars are crucial when considering the long-term dynamics of Oort cloud comets. Indeed, a synergy between galactic tides and passing stars is at work. The galactic tides generate dynamics that is quasi-integrable; hence, for a comet in the Oort cloud, one can know from the beginning whether this comet can reach the observable region, i.e., less than 5 au from the Sun, or not. The region containing such observable comets is analytically defined and has been called the Tidal Active Zone (TAZ) in Fouchard et al. (2011). Without the influence from stars, the TAZ gets depleted in approximately 2 Gyr, and the flux of observable comets reaches an anemic level. Including the effect of the stars, the TAZ remains filled at approximately 80%, as the background stars guarantee a constant flux, even at 5 Gyr. However, a single massive star is able to completely fill the TAZ, generating an increase in the flux of approximately 20% for several hundred million years.

In Fouchard et al. (2007), passing stars were shown to contribute to the flux of observable comets during the last orbital period of the comets. That is, considering only the galactic tide, a comet could be directly injected into the observable region, i.e., its perihelion distance could jump the so-called Jupiter–Saturn barrier, if its semimajor axis was larger than approximately 24000 au. The contribution of stars decreases this threshold, and comets exhibiting a semimajor axis of approximately 20000 au could also jump the barrier.

Clearly, the above process considers only background stars. However, it is well known from Hills (1981) that a rare but very close stellar encounter can produce a comet shower, which can cause a significant increase in the flux of observable comets. In this case, even comets with semimajor axes much smaller than 20000 au (the inner Oort cloud) can be observed.

2.2 Formation

The main models of the Oort cloud formation are based on the assumption that comets are residuals left after the formation of planets. Fernández (1980) and Fernández and Ip (1981) showed that bodies starting out in the outer planetary region can evolve under the combined action of planetary and stellar perturbations into Oort-cloud-type orbits. Then, Duncan et al. (1987) investigated the problem of the formation of the Oort cloud in more detail, adding galactic perturbations. To save computing time, DQT87 began their simulations with comets on low-inclination but highly eccentric orbits in the region of the giant planets. Dones et al. (2004) repeated the study of DQT87, starting with comets with semimajor axes between 4 and 40 au and initially small eccentricities and inclinations. Emel'yanenko et al. (2007) investigated a broadly similar model but with more eccentric initial orbits, motivated by the orbital distribution in the scattered disk. They found that there is no sharp boundary between the Oort cloud and the trans-Neptunian zone. The family of trans-Neptunian objects, moving along high-eccentricity orbits, is a mixture of the objects residing here over the lifetime of the Solar System and the objects visiting the Oort cloud during their dynamical history (Emel'yanenko et al. 2007, 2013).

Fernández (1997) and Fernández and Brunini (2000) studied the formation of the cloud while the Solar System was still in the stellar cluster into which it was born. Such formation processes have been further developed, considering a more realistic cluster, as an embedded cluster was invoked to produce an object such as Sedna (Brasser et al. 2006, 2008; Kaib and Quinn 2008).

Being even more realistic, Brasser et al. (2007) considered that because the lifetime of the cluster is shorter than that of the gas disk in the Solar System, the gas drag on small bodies also needs to be considered. Such a drag does not affect large objects such as Sedna, but does make it very difficult to place cometary-sized objects in a proto-Oort cloud. In addition, whereas the above process produced an inner shell, i.e., at less than 1000 au to the Oort cloud, quite easily, it was very difficult to produce an Oort cloud that extended beyond 10000 au, even in four billion years.

Consequently, the Oort cloud beyond 10000 au seems to have been formed after the gas dissipation. Then, the Nice model (Tsiganis et al. 2005) showed that a late migration of the giant planets is a natural consequence of the presence of a massive planetesimal disk beyond the young giant planets that had just formed. Such a migration would occur after the gas dissipation; then, it would be possible to build an external Oort cloud in this second step in an efficient way. This second step has been modeled in Brasser and Morbidelli (2013); Nesvorný et al. (2017) and Vokrouhlický et al. (2019) to deduce the final flux of observable comets for the three main different families: long-period, Jupiter-family, and Halley-type comets.

Consequently, it seems that both the stellar cluster and giant planets, with the help of the migration process, have contributed to the formation of the Oort cloud. However, it is difficult to evaluate the exact role of each process. In the cluster, the directions of the encounter velocities between the Sun and other stars are isotropic. Consequently, actions on the planetesimal disk would serve to increase the inclination of the objects. Higuchi and Kokubo (2015) showed that the timescale to obtain an isotropic distribution in e, i, and ω by stellar perturbations is similar to that for the lifetime of the Oort cloud (the timescale for ejection), although the timescale that the inclination distribution requires to relax is approximately three orders of magnitude shorter. As such, the comets that would be placed in the inner shell of the Oort cloud would also have large inclinations. The larger the inclination is, the weaker the scattering by the giant planets would be during their late migration.

Nordlander et al. (2017) showed that to dissipate quickly, the initial cluster should not have been too dense. Thus, it seems that for the two-step formation process to work well, the stellar cluster where the Sun was born should have a low density of stars, and this is required to explain the presence of objects like Sedna. Meanwhile, the Oort cloud itself is mainly produced by perturbations of the giant planets. In this hypothesis, the Oort cloud should contain a fingerprint of this formation process, that is, the presence of an Oort disk.

Consequently, the detection of any fingerprint of the presence of an Oort disk will give us a hint regarding the processes that were in operation during the formation of the outermost part of the Solar System. Such a fingerprint should be detected in the data available from the sample of observable comets. Fouchard et al. (2018) showed how a memory of the initial shape of the Oort cloud can be kept throughout the transport of comets until the comets reach the observable region. In the present study, we focus on the detection of the fingerprint of an Oort disk, using the same data as in Fouchard et al. (2018).

3 Observable comets

3.1 Simulations

Our analysis is restricted to the sample of comets for which the original semimajor axis is larger than 10^4 au and with a perihelion distance smaller than 5 au. For such comets, fading can be neglected because the probability of ejection from the Oort spike when the perihelion

is smaller than 5 au is higher than 80%, and for a perihelion smaller than 3 au, it is higher than 90% (Fouchard et al. 2013).

Our working samples come from the simulations performed in Fouchard et al. (2018). In this study, we performed the propagation of two different proto-Oort clouds for 4.5 Gyr under the influences of the Galactic tides, passing stars, and planets. The different sets were as follows:

- Disk-like proto-Oort cloud, named the disk model: Uniform distributions were used for orbital energy $z_i = -1/a_i$ for semimajor axis a_i between 500 and 20000 au, with the perihelion distance q_i between 3 and 50 au, ecliptic inclination i_{E_i} between 0° and 20°, and the ecliptic argument of perihelion ω_{E_i}, longitude of the ascending node Ω_{E_i}, and mean anomaly M_i all between 0° and 360°. The total number of objects for this set is 13428570.
- Isotropic proto-Oort cloud, named the isotropic model: Apart from eccentricity e_i, which has a law of distribution proportional to $e\,de$, with a perihelion distance q_i greater than 15 au, all the other following quantities are drawn from uniform distributions: orbital energy z_i for semimajor axis a_i between 500 and 50000 au, $\cos i_{G_i}$ between −1 and 1 where i_{G_i} is the galactic inclination, and the galactic argument of perihelion ω_{G_i}, galactic longitude of the ascending node Ω_{G_i}, and mean anomaly M_i all between 0° and 360°. For this set, the total number of objects is 20307700.

The comets are injected randomly into the proto-Oort cloud with an initial time between 0 and 250 Myr. Then, five final snapshots separated by 250 Myr between 3.5 and 4.5 Gyr are considered. After each snapshot, a "quiescent" propagation lasting 30 Myr takes place, where all stars that might have produced a cometary shower are removed. A comet is observable if its first passage at perihelion after the end of the quiescent period is at less than 5 au. More details concerning the simulations can be found in Fouchard et al. (2018).

Considering the original orbital elements at the previous perihelion passage before a comet becomes observable, these comets can be classified into four classes, namely jumper, creeper, KQ (Kaib–Quinn) jumper, and KQ creeper, with the following definitions: A comet is considered a *jumper* if it was beyond 10 au at the previous perihelion passage; otherwise, it is a *creeper*. In addition, it is a KQ comet if its original orbital energy increased by more than 10^{-5} au^{-1} between the previous perihelion passage and the perihelion where the comet is observable.

Distinguishing among these four scenarios in which a comet becomes observable became necessary from both observations and numerical experiments. Indeed, historically, it was first considered that for a comet to be observable, its perihelion distance had to jump the so-called Jupiter–Saturn barrier. This barrier is the region where the typical perturbation originating from the giant planets is higher than the orbital energy of the Oort cloud comets, such that the comets passing through this region are likely ejected from the Oort cloud. This observation was already made by Oort and led him to conclude that many long-period comets were "new."

The Jupiter–Saturn barrier is mainly defined by the perihelion distance and is usually considered to be a value between 10 and 15 au (Fernández 1981; Duncan et al. 1987). However, it appears from both simulations (Fouchard et al. 2017, 2018; Vokrouhlický et al. 2019) and observations (Dybczyński and Królikowska 2011) that approximately half of the observable (or observed) comets passed inside the Jupiter–Saturn barrier at their previous perihelion.

Consequently, a significant part of the observable comets did not jump the barrier but rather had their perihelion creep across the Jupiter–Saturn region.

Kaib and Quinn ([2009](#)) showed that for a majority of observable comets, their orbital energy received a kick from the planetary perturbations at the previous perihelion passage, increasing their orbital energy. This kick was crucial for observability because it made the effect of the galactic tides stronger, such that the perihelion distance could reach the observable region in a single orbital period.

The statistical properties of these four different classes are significantly different (Fouchard et al. [2018](#)). Here, their main properties are presented, considering the original orbital elements at the perihelion where the comets are observable.

– Jumper: No preference between prograde and retrograde orbits with a nearly flat galactic longitude of the ascending node. These comets come from the outermost part of the cloud with a median original semimajor axis of approximately 36500 au.
– KQ jumper: A preference for prograde orbits, 58% and 66% for the disk-like and isotropic models, respectively. The original semimajor axis is still quite large, i.e., a median value of approximately 30000 au.
– Creeper: Preference for retrograde orbits (68% and 72% for the disk and isotropic models, respectively) and a much smaller original semimajor axis with median values of approximately 18500 au and 16000 au, respectively.
– KQ creeper: As with creepers, a significant preference for retrograde orbits (56% and 67%, respectively) at a moderate original semimajor axis (median value of approximately 22000 au for both models).

However, if different classes of comets have different statistical properties, Fouchard et al. ([2018](#)) suggest that these properties of the current orbits would be quite independent of the model used: disk or isotropic. The detection of a "memory" of the initial shape was much easier considering the original orbital elements at the perihelion passage preceding the perihelion where the comets are observable.

Thus, the present study aims to optimize a method to highlight the signature of the initial and/or present shape of the Oort cloud. Because we are mainly interested in the signature of an initial disk, we now focus on the disk model. In addition, in Fouchard et al. ([2018](#)), KQ creepers and creepers appear to share almost the same properties; hence, for simplicity, we merge these two classes. From now on, if not specified, the orbital elements of a comet always refer to the original orbital elements at the previous perihelion passage before the comet is observable.

3.2 Long-term behavior of observable comets for the disk model

We wish to understand in detail how the "memory" of the proto-disk shape is propagated until the comets become observable. We consider the long-term evolution of comets for the age of the Solar System. For such an investigation, in the simulations made in Fouchard et al. ([2018](#)), the positions of all comets have been stored every 250 Myr from $t = 0$ yr.

After an investigation of the data, five long-term behaviors have been identified:

B1: The perihelion distance and ecliptic inclination remain almost constant during the entire integration, except at the very end when the perihelion distance decreases abruptly to reach the observable region.
B2: The ecliptic inclination and the galactic longitude of the ascending node are nearly constant, whereas the perihelion distance performs an almost full galactic cycle until it returns to the planetary region just before becoming observable.
B3: The perihelion distance and the galactic inclination perform a full galactic cycle, whereas the galactic longitude of the ascending node performs a half period.

B4: More than one perihelion distance cycle is performed.

B5: All remaining cases.

Clearly, the first three long-term behaviors are strongly related to the evolution of a signature of an initial disk shape. B1 and B2 are more typical of KQ jumpers as the ecliptic inclination is almost constant during the entire time span, and as is well known, KQ jumpers have a preference for prograde orbits.

However, B2 long-term behavior is dynamically very different from that of B1. In particular, B1 long-term behavior corresponds mainly to relatively stable orbits, and B2 long-term behavior corresponds to comets for which the perihelion cycle is close to the separatrix between the librating and circulating motion of the galactic argument of the perihelion (Heisler and Tremaine 1986; Higuchi et al. 2007). For such orbits, the galactic longitude of the ascending node and the galactic inclination appear to remain mainly constant during the entire perihelion cycle, except when the perihelion distance passes through its minimum. However, the galactic longitude of the ascending node does experience a small decrease for comets close to the ecliptic plane (Higuchi et al. 2007).

The B3 behavior is explained by the following. The galactic inclination and galactic argument of the perihelion exhibit the same period cycle as the perihelion distance (Heisler and Tremaine 1986). However, the period of the galactic longitude of the ascending node Ω_G is approximately twice this period (Higuchi et al. 2007). Thus, starting from an orbit aligned with the ecliptic, after one full cycle of the galactic inclination, Ω_G has performed only half of a cycle. This implies that for such an orbit, the ecliptic inclination would be approximately 2η, where η is the inclination of the galactic plane with respect to the ecliptic. Hence, after one full cycle of the perihelion distance, the ecliptic inclination is approximately 120°, which is a favorable ecliptic inclination for creeper comets.

The B4 behavior is typical of a high semimajor axis, whereas B5 represents unclassifiable behaviors.

Numerically, the identification of these behaviors was not easy; nevertheless, the following strategy has been optimized empirically. Indeed, because of the passing stars, we cannot assume that the quasi-integrability of the action of the galactic tides applies to any particular property. Thus, the focus is placed on the main characteristics of each behavior. First, we need to detect when a galactic cycle of the perihelion distance has been accomplished. For the disk model, initially, the perihelion distance is near its minimal value with an eccentricity greater than 0.9. A cycle is achieved when the eccentricity reaches a minimum and then returns to a maximum. However, to detect only significant cycles, thresholds had to be placed on the extremal values of the eccentricity, i.e., the minimum should be smaller than 0.89 and the maximum should be higher than 0.91.

Thus, B1 corresponds to the absence of a galactic cycle, and the orbit always remains prograde; otherwise, if some cycles have been detected and the orbit is always prograde, then it is classified as a B2 long-term behavior (usually only one cycle is detected). If one and only one shift from prograde to retrograde has been detected, then it is a B3 long-term behavior (again, usually one perihelion cycle is evident). For all other cases, if at least two perihelion cycles have been detected, then it is a B4 long-term behavior; otherwise, it is a B5 long-term behavior. Note that the original orbital elements when the comet is observable are not considered for the determination of long-term behaviors. Indeed, during the last orbital period, abrupt changes in the orbital elements may occur, leading to missed detection of the long-term behavior.

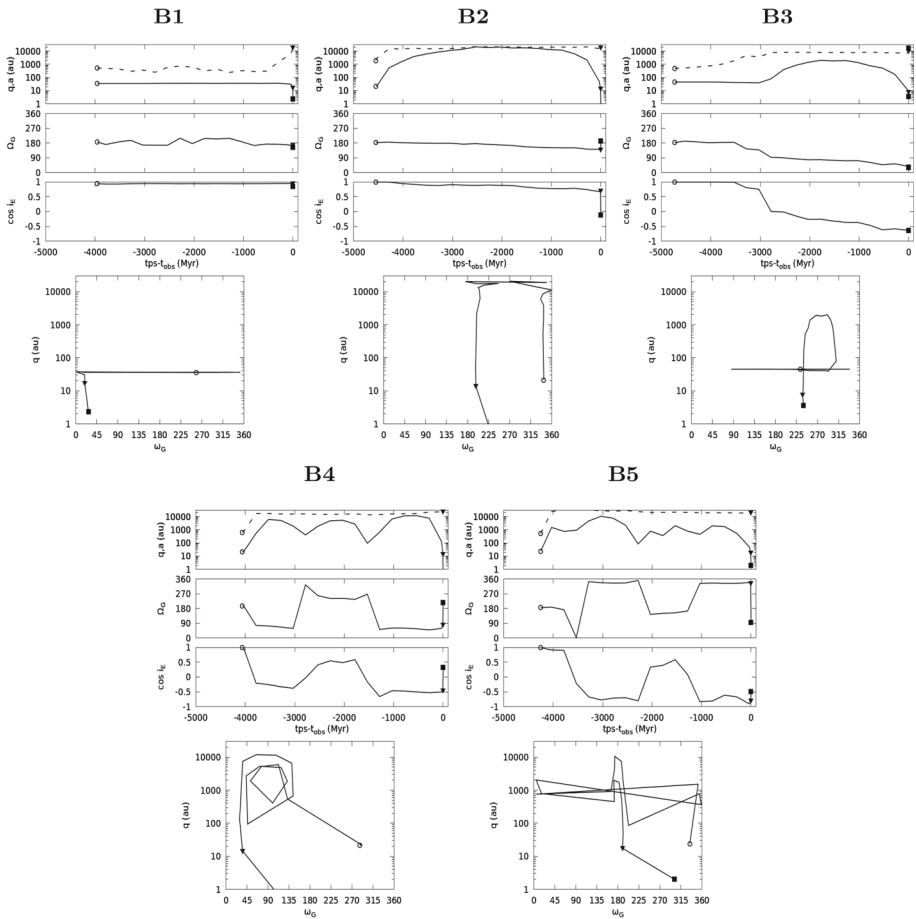The different long-term behaviors are illustrated in Fig. 1.

Fig. 1 Long-term evolution of observable comets. The time is given in million years before the time of observation. The open circles correspond to the initial position, the downward filled triangles correspond to the original orbit at the perihelion preceding the observation, and the filled squares correspond to the original orbit when the comet is observable. The evolution is given by one point every 250 Myr. For each panel, from top to bottom, the evolution versus time of the semimajor axis (dashed line) and perihelion distance (full line) is displayed on the first plot, the galactic longitude of the ascending node on the second plot, the cosine of the ecliptic inclination $\cos i_E$ on the third plot, and on the bottom plot, the evolution of the perihelion distance with respect to the galactic argument of perihelion. The boldface letter above each panel refers to a long-term behavior described in the main text

3.2.1 Initial and final location according to the long-term behavior

The location of observable comets with B1, B2, or B3 long-term behaviors both initially and at the previous perihelion before the comets are observable should be considered. Figure 2 shows the distribution of the perihelion distance q and $\cos i_E$ for these two instants and the position of the comets in the (q, $\cos i_E$) plane for the three different behaviors.

With regard to B1 long-term behavior, most of the comets exhibiting this behavior initially had a perihelion distance beyond 40 au, where the classical Kuiper belt is located. In fact, B1 long-term behavior is characterized by the less dynamically evolved comets. Even at the
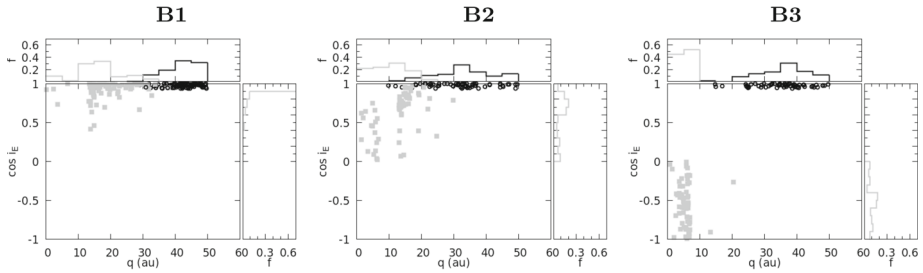
Fig. 2 For each panel, the distribution of the perihelion distance is shown in the upper plot, and the distribution of $\cos i_E$ is shown in the right-side plot. The central diagram shows the position of the observable comets in the $(q, \cos i_E)$ plane. The open black circles are for initial parameters, and the filled gray squares represent previous perihelion parameters. B1, B2, and B3 above each panel refer to the long-term behavior considered

previous perihelion distance, these comets have the smallest inclinations, typically smaller than 25°, and greatest perihelion distances, with the maximum of the distribution between 15 and 20 au.

Comets with B2 long-term behavior are in a significantly different place. Indeed, the maximum of the distribution of the initial perihelion distance is located just beyond Neptune. They are also more evolved with an ecliptic inclination at the previous perihelion ranging over the entire range of prograde orbits (by definition); however, most have inclinations between 25° and 60°.

B3 long-term behavior corresponds to the most evolved case. While their initial perihelion distances show a preference for values between 35 and 40 au, the distribution of the ecliptic inclinations at the previous perihelion spans over all retrograde orbits (again by definition) but with a preference for i_E close to 120°. The perihelion distance at the previous perihelion is almost always smaller than 10 au.

3.2.2 New definitions of the classes of long-term behaviors

First, we see how each class of comets is distributed among the different long-term behaviors.

The proportion of each long-term behavior is given in Table 1. In addition, for each long-term behavior and class, a mean orbital energy z_m of approximately 530 Myr before a comet is observable is computed. For clarity, the last column of the table gives the semimajor axis that corresponds to z_m, i.e., $a_m = -1/z_m$.

Clearly, B1 long-term behavior is characterized by a very small semimajor axis (approximately 1000 au), which explains why these comets evolved so weakly within the time span of approximately 4 billion years. It is well known that the perihelion cycle is related to the orbital energy of the comet (Breiter and Ratajczak 2005; Higuchi et al. 2007). In particular, the minimal period cycle is given by

$$P_q = \frac{\pi}{2\sqrt{5}k\rho_\odot P},$$

where k is the universal gravitational constant, $\rho_\odot$ is the density of the galactic disk in the solar neighborhood, and P is the Keplerian period of the comet. At $a \approx 1000$ au, this minimal value is approximately 50 Gyr, much longer than the age of the Solar System. Thus, B1 comets were frozen from the beginning and became observable only because of dynamical processes at work at the very end of their evolution. In particular, the increase in the orbital energy helps the tides to inject the perihelion distance inside the observable region.

Table 1 For each class of observable comets, the number (second column) and proportion (third column) of comets with long-term behaviors stated in the first column are shown

	N	Proportion (%)	$a_m = -1/z_m$
Jumpers (95.9 comets Myr^{-1})			
B1	15	2.5	976.9
B2	11	1.6	5021.2
B3	71	10.1	4330.6
B4	635	75.5	30221.6
B5	104	10.3	13094.2
Creepers (97.5 comets Myr^{-1})			
B1	13	4.0	1121.7
B2	67	20.3	7068.2
B3	108	35.8	7621.5
B4	95	32.6	18800.0
B5	24	7.3	10466.8
KQ jumpers (97.5 comets Myr^{-1})			
B1	100	26.6	979.4
B2	98	33.4	6545.0
B3	19	6.7	9888.0
B4	87	28.2	15683.0
B5	15	5.1	11313.7

The last column gives the semimajor axis in au corresponding to the mean orbital energy of the comets in each subset. The observable flux of each class is also given

The comets with B2 long-term behavior are such that $a_m \approx 7000$ au for the creepers and KQ jumper classes. This corresponds to a minimum period of the perihelion distance cycle equal to 2.7 Gyr. Clearly, these comets are more evolved than comets with B1 long-term behavior. In fact, with this value as a minimal value, it is clear that these comets have performed a full galactic perihelion cycle. Similar values are evident for the creepers with B3 long-term behaviors.

Comets with the B4 long-term behavior have a semimajor axis of at least 15000 au (for the KQ jumpers) and yield a minimum period of the perihelion distance cycle equal to 0.8 Gyr. Clearly, in this case, several cycles are allowed.

As already mentioned, only B1, B2, and B3 are long-term behaviors related to the initial disk shape of the Oort cloud. As presented in Table 1, B1 and B2 are typical of KQ jumpers, whereas B3 is typical of creepers.

Consequently, we would like to maximize the influence of B1 and B2 for the KQ jumper class and the influence of B3 for the creeper class. The only parameter we can change is the limiting value of the perihelion distance used to define the creepers. Thus far, this value is taken to be equal to $q_c = 10$ au. Figure 3 shows the evolution of the proportions of B1+B2 and of B3 in creepers and KQ jumpers, versus q_c, with q_c ranging from 5 au to 21 au.

From this figure, the proportion of B3 long-term behaviors is maximal among the creepers for $q_c = 7$ au, and the proportion of B1+B2 long-term behaviors is maximal among the KQ jumpers for $q_c = 13$ au. These maxima correspond to the minima of B2+B3 and B1 long-term behaviors, respectively.

Using these data, we can make new definitions for the classes. Let q_p be the perihelion distance at the perihelion preceding the observation of a comet and Δz be the variation of
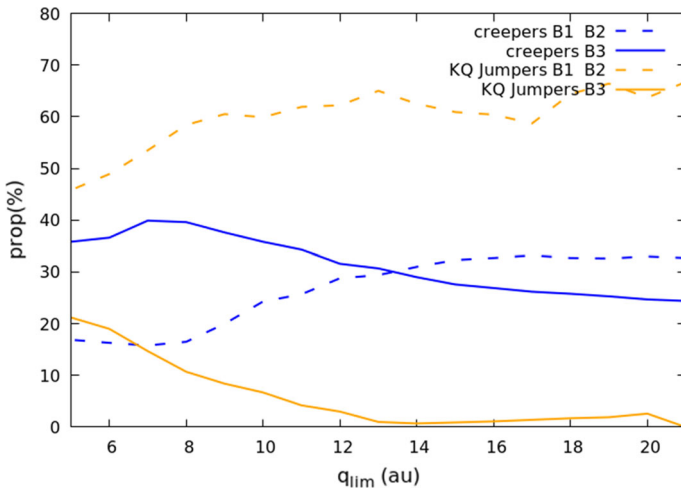
Fig. 3 Proportion of comets with a specific long-term behavior for the creepers and KQ jumpers versus the threshold limit q_c used to separate the two classes. The meaning of each line is given in the upper right key

	N	Proportion (%)	$a_m = -1/z_m$
Table 2 Same as Table 1 but for the new definition of creepers, KQ creepers, and mixed class of comets			
Creepers (56.3 comets Myr^{-1})			
B1	4	2.9	1031.9
B2	18	12.9	7564.6
B3	58	39.9	7423.1
B4	47	35.7	19,080.8
B5	14	8.6	10,558.5
KQ jumpers (32.1 comets Myr^{-1})			
B1	84	38.6	934.7
B2	45	26.4	8675.8
B3	2	1.0	4066.4
B4	53	30.4	15,854.4
B5	7	3.6	16,875.0
Mixed (76.1 comets Myr^{-1})			
B1	28	8.0	1252.6
B2	104	31.6	6146.3
B3	77	23.8	8387.9
B4	103	30.3	18,673.7
B5	21	6.3	8063.7

the original orbital energy between these two perihelion passages. If $q_p < 7$ au, then the comet is a creeper; if $q_p > 13$ au, then it is a jumper, and if $\Delta z > 10^{-5}$ au^{-1}, then it is a KQ jumper. Comets with $7 < q_p < 13$ au belong to a new mixed class. From now on, we consider these new definitions for the observable comet classes.

Table 2 presents the proportion of long-term behaviors in creepers, KQ jumpers, and mixed classes of comets. The numbers of comets in each class are lower; however, the proportion of

B3 (resp. B2) long-term behaviors among creepers (resp. KQ jumpers) is higher than before. For the mixed class, one notes that B2 long-term behavior dominates, with a significant proportion of B3 long-term behaviors.

3.3 Fingerprints

Figure 4 shows the distribution of Ω_{G_p} and $\cos i_{E_p}$, where Ω_{G_p} and i_{E_p} are the galactic longitude of the ascending node and ecliptic inclination at the previous perihelion, respectively, for the jumpers, creepers, KQ jumpers, and mixed class comets for our two different models. The position of each observable comet in the $(\Omega_{G_p}, \cos i_{E_p})$ plane is also shown.

The following observations can be made from Fig 4:

- The jumper classes are very similar for both the disk and the isotropic models. The observable comets are almost uniformly spread along the $i_G = 90°$ line, where i_G is the galactic inclination. As explained in "Appendix B," this is expected because at the previous perihelion, the perihelion distance is strongly decreasing, which means that the strength of the tides is high; thus, $\sin i_{G_p}$ is close to unity.
- The situation is different for the creeper class. For both models, creepers have a preference for retrograde orbits. This was already observed in previous studies (Fouchard et al. 2017, 2018), and it is easily explained by the simple fact that creepers have to avoid being scattered by Jupiter or Saturn. This should naturally produce a maximum of the $\cos i_{E_p}$ distribution at approximately -1, as observed for the isotropic model. However, this maximum is approximately at -0.5 for the disk model. This is precisely the expected preference value when a significant proportion of comets have B3 long-term behavior.
- For the KQ jumpers, it is more difficult to disentangle what is related to the class of the comets and what is related to a fingerprint of the initial shape. Indeed, for both the disk and isotropic models KQ jumpers have a preference for prograde orbits. However, this preference is much stronger for the disk model with 64% of the comets having $\cos i_{E_p} > 0.75$, whereas 45% of comets for the isotropic model satisfy this condition. In addition, because the KQ jumpers class for the disk model contains mainly B1 long-term behaviors, that class corresponds to poorly dynamically evolved comets with 79% of the comets satisfying the condition $\Omega_{G_p} \in [135°, 225°]$, whereas this proportion is approximately 55% for the isotropic model.
- The case of the mixed class is interesting. Indeed, for the disk model, one clearly sees the effect of B2 long-term behavior, which is very similar to the signature of B1 long-term behavior in the KQ jumpers but for more-evolved comets. Consequently, the distribution of Ω_{G_p} is more spread toward lower values, and the maximum of the $\cos i_{E_p}$ distribution is between 0.5 and 0.75 and, hence, detached from the ecliptic plane. In addition, the influence of B3 long-term behaviors is also evident with a second maximum of the $\cos i_{E_p}$ distribution at approximately -0.5. On the Ω_{G_p} distribution, Ω_{G_p} is mainly spread in the $[0, 180°]$ range. These features are directly related to the initial shape and are not present for the isotropic model. Indeed, the only clear feature that is still detectable in the distributions is the preference for retrograde orbits, which is related to the minimum of the Ω_{G_p} distribution around 180°.

Consequently, the fingerprints of the initial shape are clearly seen in the different distributions obtained from the observable comets. However, we are here in the best situation where all the necessary data have been stored during the numerical propagation of the comets. What happens now when this is not the case?
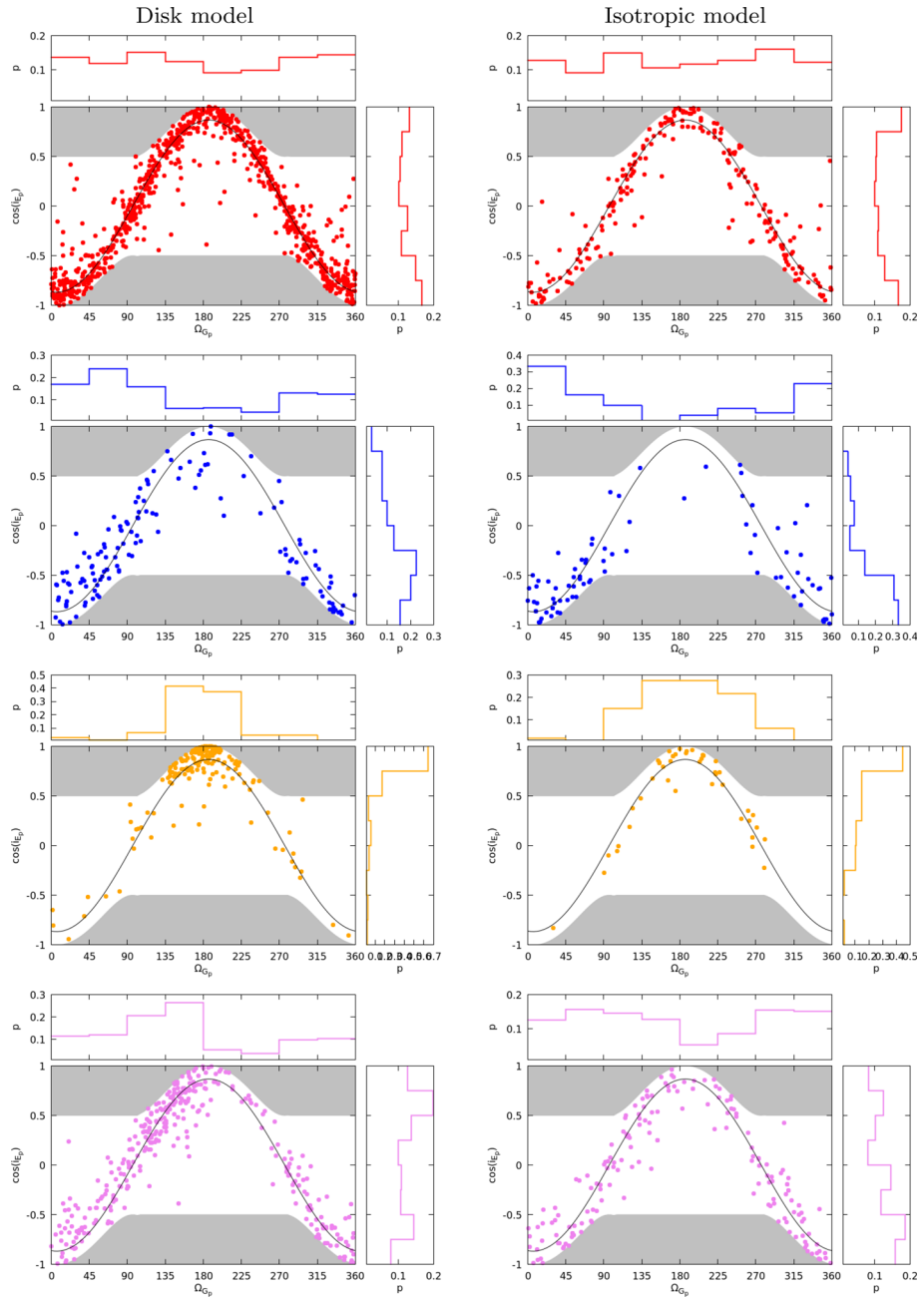
Fig. 4 Position of the observable comets in the $(\Omega_{G_p}, \cos i_{E_p})$ plane and distributions of Ω_{G_p} (above each panel) and $\cos i_{E_p}$ (right side of each panel), where Ω_{G_p} and $\cos i_{E_p}$ are the galactic longitude of the ascending node and ecliptic inclination at the previous perihelion. From top to bottom, the panel represents jumpers (in red), new creepers (in blue), new KQ jumpers (in orange), and mixed class (in violet). The left column is for the disk model, and the right column is for the isotropic model. The gray area is a forbidden region, and the black curve corresponds to $i_G = 90°$, where i_G is the galactic inclination (see "Appendices A and B," respectively, for details)

3.4 Fingerprints with reconstructed orbits

A double problem arises when one has to deal with real data. In our simulations, the original orbital elements at the previous perihelion are just stored during the propagation. Thus, it is easy to determine the class of an observable comet. When one considers real data or data originating from other simulations, one does not have access to the previous orbital elements. The second problem is that the uncertainties on the original orbital elements of known comets may be large, in particular for the original orbital energy, which plays a key role in the determination of the previous perihelion distance.

It is not within the scope of the present paper to handle real data and evaluate how these uncertainties can affect the results. Such uncertainties are very comet and catalog dependent. Hence, the strategy we use to work with real data is postponed to a forthcoming paper.

Regarding the first problem, the only possible strategy to overcome this is to perform a backward integration from the original orbit of the observable comets over one orbital period, considering only the galactic tides. The orbital elements obtained are called the reconstructed orbital elements. The reconstructed orbital elements are different than the previous orbital elements in integration with passing stars included . This is particularly true for the orbital energy. Indeed, for the previous orbital elements, the original orbits were considered, i.e., the orbits before planetary scattering when the comets pass through perihelion. Clearly, it is not possible to retrieve the planetary scattering, which mainly affects the orbital energy, at the previous perihelion for the reconstructed orbits. However, we can still consider that at least for the perihelion distance, ecliptic inclination, argument of perihelion, and longitude of the ascending node, we obtain a good approximation of the correct values. Obviously, for some comets it will not be the case but this should not affect the statistics.

For instance, considering the previous perihelion distance, which is a key parameter in determining the class of a comet, the difference between the true previous perihelion distance q_p and reconstructed one q_r versus q_p is shown in Fig. 5.

According to this figure, the error on the reconstructed perihelion distance appears to grow nearly linearly with perihelion distance, with most of the errors between $q_p/10$ and q_p. Thus, as observed in the figure, the reconstruction of the previous perihelion distance is more reliable for creepers and mixed class comets, rather than for KQ jumpers and jumpers.

What about the KQ process? As already mentioned, it is completely hopeless to estimate the planetary kick received by the comets during their previous perihelion passage. However, one knows that for KQ jumpers, the kick was given by Uranus and Neptune. Hence, if the previous perihelion was greater than 32 au, then it is very unlikely that the comet is a KQ one. In addition, in the simulations, most non-KQ jumpers have their previous perihelion much further than Neptune's orbit.

Consequently, instead of classes, four ranges of the reconstructed previous perihelion distance are considered: $q_r < 7$ au (zone 1), $7 < q_r < 13$ au (zone 2), $13 < q_r < 32$ au (zone 3), and $q_r > 32$ au (zone 4). The proportion of comets in each zone for the disk model is 28%, 27%, 23%, and 22%. Hence, our sample of observable comets is shared in subsets of almost the same size.

Table 3 provides the general statistics regarding the filling of the four zones defined above with respect to the class of the comets (which are known because the comets are coming from simulations). First of all, the filling of each zone by a different class is nearly independent of the model. This is expected because the uncertainty comes from the passing stars, which are independent of the model used. Creepers are mainly concentrated in zone 1 (more than 70% of comets in this zone are creepers), and zone 4 contains almost only jumpers (more than 90%). Zone 2 is also filled by more than 70% of mixed class comets. The problematic
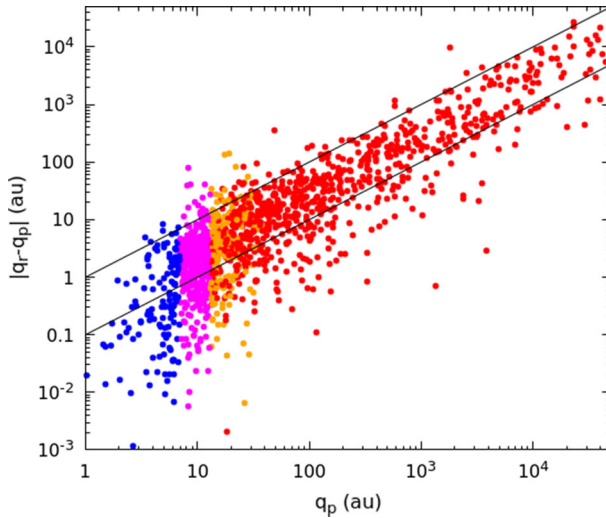
Fig. 5 Difference between the true previous perihelion distance q_p and the reconstructed one q_r versus q_p. Jumpers, KQ jumpers, creepers, and mixed class comets are shown by red, orange, blue, and magenta dots, respectively. The two full lines correspond to $|q_r - q_p| = q_p$ and $|q_r - q_p| = q_p/10$

Table 3 For both models, isotropic and disk models give the proportion of comets (in percent) in each zone, according to their reconstructed perihelion distance

Zone	Jumpers	Creepers	KQ jumpers	Mixed
Disk model				
Z1	2.50	71.89	2.59	23.02
Z2	11.86	7.36	9.99	70.78
Z3	46.13	0.58	33.68	19.61
Z4	91.27	0.00	7.75	0.98
Isotropic model				
Z1	2.39	71.43	1.34	24.84
Z2	9.67	4.89	6.69	78.75
Z3	44.75	2.73	26.93	25.58
Z4	93.88	0.00	2.93	3.20

zone is zone 3, which should contain mainly KQ jumpers, whereas approximately 45% of comets in this zone are jumpers, versus 27 and 33% of KQ jumpers for the disk and isotropic models, respectively. This problem comes from the facts that the error on the reconstructed perihelion distance is larger than approximately 10 au and it is impossible to detect the KQ effect.

However, the distributions of the two most interesting orbital elements, that is, the cosine of the ecliptic inclination $\cos i_E$ and the galactic longitude of the ascending node Ω_G, are essentially flat for jumpers (Fouchard et al. 2018). Thus, one can hope that the high proportion of jumpers in zone 3 will not erase the fingerprint coming from an Oort disk.

This is what we can check in Fig 6, which shows the distributions of $\cos i_{E_r}$ and Ω_{G_r} for the observable comets in the different zones and for the two models. For the disk model, the fingerprints related to the initial disk shape already observed in Fig. 4 are surprisingly well reproduced in zone 1 (creepers) and zone 2 (mixed class). In zone 3, the concentration of
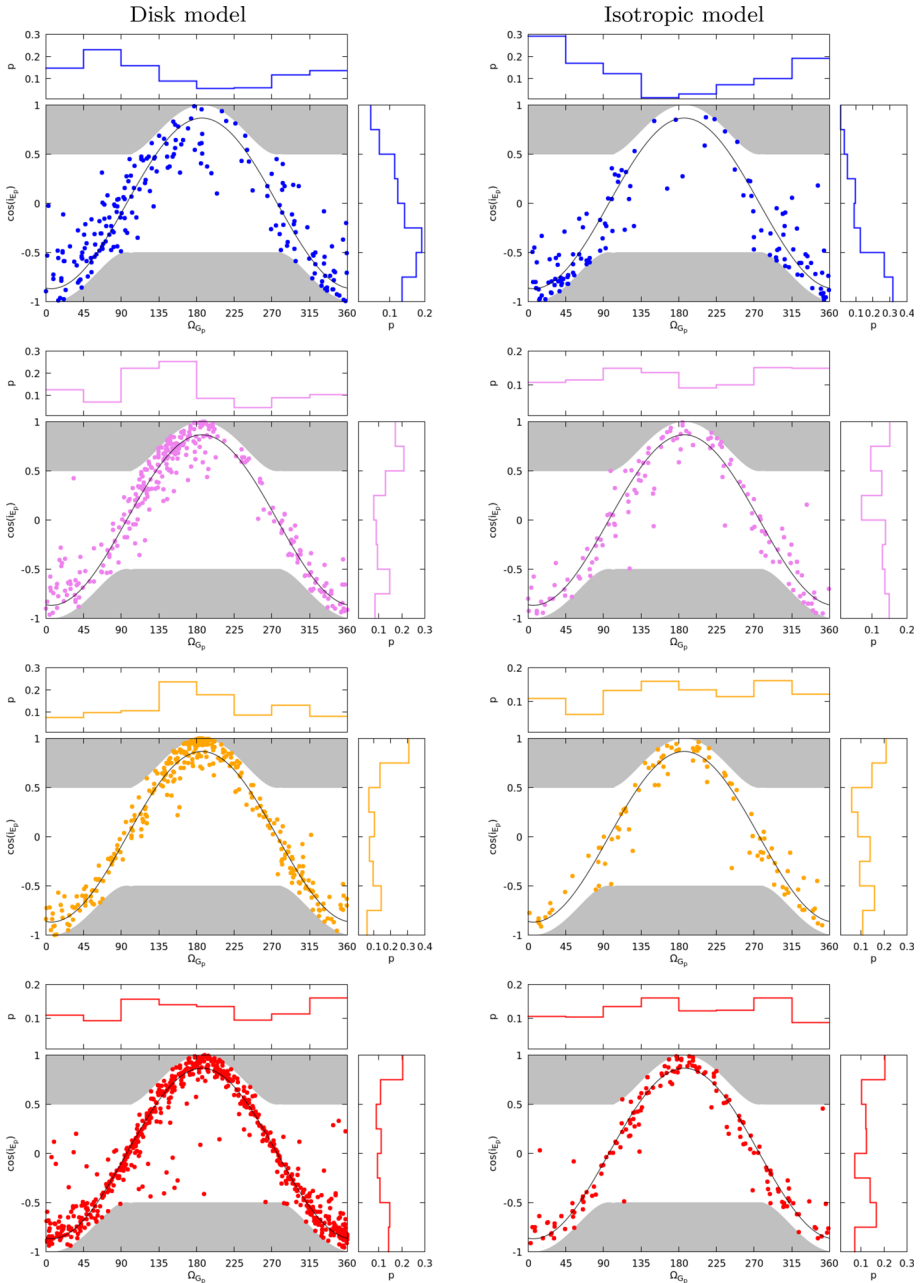
Fig. 6 Same as Fig. 4 but for the four different zones of the reconstructed previous perihelion distance. From top to bottom, the panels are for zone 1 ($q_r < 7$ au), zone 2 ($7 < q_r < 13$ au), zone 3 ($13 < q_r < 32$ au), and zone 4 ($q_r > 32$ au)

the orbits toward the ecliptic is still observed; however, such concentration is also related to the KQ jumper class, regardless of the initial shape. Hence, this feature seems to be less adequate for the detection of an initial Oort disk fingerprint.

Looking at the isotropic model, in zone 1, the same features are observed as that for the creepers class of this model. For zone 2, the distribution is now nearly flat, and even the preference for retrograde orbit is not as evident as for the mixed class comets of this model. Similarly for zone 3, with less data, the "noise" introduced by the jumpers in this zone is higher than the signal coming from the KQ jumper class.

In general, it seems that working with reconstructed orbits does not kill the fingerprints of an initial proto-Oort disk.

4 Conclusions

From the pioneer work of Jan Oort, little attempt has been made on the use of the observed data to retrieve information concerning the Oort cloud, its structure, and its formation. Our group aims to use the flux of long-period comets to retrieve information regarding the initial shape of the Oort cloud. This task is not easy, and each step involved in the process needs to be optimized. In Fouchard et al. (2018), we showed that a memory of the Oort cloud was propagated and detectable in the flux of observable comets. However, it was not clear how this memory was propagated. In addition, it was not clear whether the fingerprints observed could persist when applied to real data.

Using the same numerical data as Fouchard et al. (2018), we showed in the present study that the memory of an initial disk shape of the Oort cloud is propagated through three main long-term behaviors:

- B1 comets maintain a small semimajor axis, approximately 1000 au, during their evolution. At the end, a significant increase in the semimajor axis provides strength to the galactic tides, allowing the injection of the perihelion distance into the observable region.
- B2 refers to comets whose perihelion distance has performed an almost full galactic cycle, whereas $\cos i_G$, where i_G is the galactic inclination, and the galactic longitude of the ascending node Ω_G remained nearly constant. Such behavior is usually found when the evolution of the galactic argument of perihelion is near the separatrix between the librating and circulating motion.
- B3 corresponds to comets whose perihelion distance and $\cos i_G$ have performed a full galactic cycle, whereas Ω_G has achieved only a half cycle. This naturally leads to a final ecliptic inclination i_E near 120°, .

Special attention should be paid to the evolution of Ω_G. Starting with orbits with small ecliptic inclinations means that initially Ω_G is close to the galactic longitude of the ascending node of the ecliptic plane, i.e., 186°. On such orbits, the action of the galactic tides induces a decrease in Ω_G. Thus, comets with B1 behavior had Ω_G close to its initial value, comets with B2 behavior showed a moderate departure from 186° to smaller values, and for comets with B3 behavior, Ω_G showed a peak located at approximately 60°.

We showed that observable comets with different long-term behaviors become observable through different processes even for their ultimate orbital period. Indeed, we defined four classes of comets, considering the previous perihelion distance q_p of the comets and the variation Δz of their original orbital energy during the last orbital period. Comets with $q_p < 7$ au, called creepers, mainly exhibit B3 long-term behavior; comets with $7 < q_p < 13$ au, called mixed class, mainly exhibit B2 and B3 long-term behaviors; and comets with $q_p > 13$ au and $\Delta z > 10^{-5}$ au^{-1}, called KQ jumpers, mainly exhibit B1 and B2 behaviors. All other comets, called jumpers, mainly have at least two detectable galactic perihelion cycles.

Considering the distributions of $\cos i_E$ and Ω_G at the previous perihelion distance, we were able to detect the following fingerprints of the initial disk:

- For the creeper class, a maximum of the $\cos i_E$ distribution at approximately -0.5, i.e., 120°, is observed. This is typical of B3 long-term behavior, whereas it should be at -1 for a typical creeper class.
- For the mixed class, a global maximum of the $\cos i_E$ distribution is at 0.5–0.75, typical of B2 long-term behaviors, and a secondary maximum is at approximately -0.5. As regards the Ω_G distribution, a strong preference was observed for values in $[0, 180°]$. All three fingerprints were absent considering the isotropic model.
- For the KQ jumpers class, a strong preference was observed for both Ω_G values close to 180° and $\cos i_E$ greater than 0.75.

For real data, we do not have access to the true q_p and even less to Δz. Hence, we have considered the reconstructed perihelion distance obtained from the backward propagation of the observable original orbit over one orbital period, considering only the galactic tides. Using only the reconstructed perihelion distance and considering zones instead of classes, we have shown that the two first fingerprints were easily detectable, and a detection of the last one was still possible.

Thus, we are ready to work with real data, and now we are able to identify which fingerprint is still detectable in a reconstruction of the previous orbital elements. However, the main problem now is the reliability of the orbits of the observed long-period comets. Is the accuracy of the present orbits of observed long-period comets sufficient to constrain the initial form of the Oort cloud by the method we described? This issue is the subject of a future paper, which is in preparation now.

A Forbidden region

The ecliptic coordinates of the Galactic pole in the North Hemisphere are $l = 180.02°$ and $b = 29.81°$; i.e., the galactic plane is inclined by $\eta = 60.19°$ with respect to the ecliptic plane. The origin of the galactic longitude Γ is located toward the present galactic center, with ecliptic coordinates of $l = 266.84°$ and $b = -5.54°$. Calling A the ascending node of the ecliptic with respect to the galactic plane, the galactic longitude of A is, thus, $L_A = 186.38°$. Consequently, an object with an ecliptic inclination close to 0° would have its galactic longitude of the ascending node close to $L_A = 186.38°$. Similarly, an object with an ecliptic inclination near 180° will have its galactic longitude of the ascending node near 6.38° (see Leinert et al. 1998, for more details on the transformations between ecliptic and galactic coordinate systems). More generally, given an ecliptic inclination, not all values of the galactic longitude of the ascending node are allowed.

Considering A as the origin for the ecliptic and galactic longitude, we note $\tilde{\Omega}_E$ and $\tilde{\Omega}_G$ as the ecliptic and galactic longitude, respectively. Using spherical trigonometry, one can show the following:

$$\tan \tilde{\Omega}_G = \frac{1}{\cos \eta} \left(\frac{\sin \tilde{\Omega}_E}{\cos \tilde{\Omega}_E + \frac{\tan \eta}{\tan i_E}} \right). \tag{1}$$
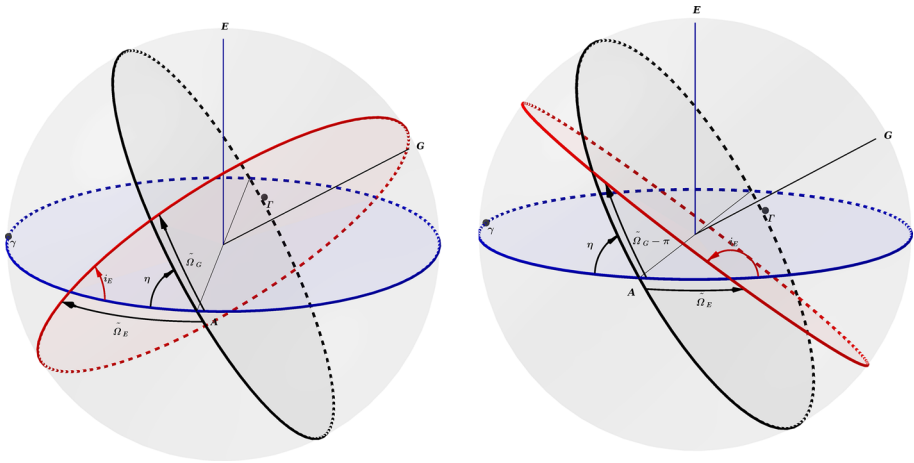
Fig. 7 Left: position of a prograde orbit with respect to the ecliptic plane and the galactic plane. Right: the same for a retrograde orbit. See text for the meaning of the angles

If $|\tan i_E| > \tan \eta$, then $\tan \tilde{\Omega}_G \to \pm\infty$ as soon as $\cos \tilde{\Omega}_E \to -\frac{\tan \eta}{\tan i_E}$. Noting that for $x \to 0$, $\sin x \sim x$, and $\cos x - 1 \sim -x^2/2$, this is also true for $|\tan i_E| = \tan \eta$ (similarly in π). Consequently, when $i_E \in [\eta, \pi - \eta]$, $\tilde{\Omega}_G$, and thus, Ω_G can take any value. If $|\tan i_E| < \tan \eta$, then $\tan \tilde{\Omega}_G$ is a bound smooth function of $\tilde{\Omega}_E$. Differentiating Eq. 1 with respect to $\tilde{\Omega}_E$, one finds that extrema are obtained when

$$\cos \tilde{\Omega}_E = -\frac{\tan i_E}{\tan \eta}. \tag{2}$$

The extreme values of $\tilde{\Omega}_G$ are then the solutions of

$$\tan \tilde{\Omega}_G = \pm\frac{1}{\cos \eta} \frac{\tan i_E}{\sqrt{\tan^2 \eta - \tan^2 i_E}}. \tag{3}$$

Let us call $\tilde{\Omega}_{E1}$ the solution such that $\tilde{\Omega}_{E1} \in [0, \pi/2[$.

As shown in Fig. 7(left), one notes that when $0 \le i < \eta$, when $\tilde{\Omega}_E = 0$ or π, $\tilde{\Omega}_G = 0$. Consequently, the range of values spanned by $\tilde{\Omega}_G$ is $[-\tilde{\Omega}_{E1}, \tilde{\Omega}_{E1}]$. Further, because $\Omega_G = \tilde{\Omega}_G + L_A$, the range for Ω_G is $[L_A - \tilde{\Omega}_{E1}, L_A + \tilde{\Omega}_{E1}]$.

Similarly, when $\pi - \eta \le i < \pi$, as shown in Fig. 7(right), one notes that if $\tilde{\Omega}_E = 0°$ or π, then $\tilde{\Omega}_G = \pi$. Thus, the range of values spanned by $\tilde{\Omega}_G$ is $[\pi - \tilde{\Omega}_{E1}, \pi + \tilde{\Omega}_{E1}]$, and the range for Ω_G is $[\pi + L_A - \tilde{\Omega}_{E1}, \pi + L_A + \tilde{\Omega}_{E1}]$.

In Fig. 4, the gray areas correspond to the forbidden regions for Ω_G.

When $0 \le i_E \le \eta$, one can compute the extreme value of i_E as a function of $\tilde{\Omega}_G = \Omega_G - L_G$. We obtain

$$\tan i_E = \frac{\sin \eta \| \tan(\Omega_G - L_G)\|}{\sqrt{1 + \tan^2 \eta \tan^2(\Omega_G - L_G)}}. \tag{4}$$

B Line $i_G = 90°$

When we consider the orbital elements of an observable comet at the perihelion preceding the passage where the comet is observable, it means that we are considering a specific time at which the strength of the action of the Galactic tides is particularly strong because the perihelion distance is quickly decreasing toward the observable region.

It is well known from Heisler and Tremaine (1986) and Matese and Whitman (1992) that the strength of the Galactic tides increases with $\sin i_G$, where i_G is the Galactic inclination. Consequently, our observable comets should have a preference for $\sin i_G$ close to one.

One can easily find, using spherical trigonometry, that $i_G = 90°$ implies that:

$$\cos i_E = -\cos(\Omega_G - 6.38°)\sin\eta. \tag{5}$$

References

Brasser, R., Morbidelli, A.: Oort cloud and Scattered Disc formation during a late dynamical instability in the Solar System. Icarus **225**, 40–49 (2013). https://doi.org/10.1016/j.icarus.2013.03.012

Brasser, R., Duncan, M.J., Levison, H.F.: Embedded star clusters and the formation of the Oort cloud. Icarus **184**, 59–82 (2006). https://doi.org/10.1016/j.icarus.2006.04.010

Brasser, R., Duncan, M.J., Levison, H.F.: Embedded star clusters and the formation of the Oort cloud. II. The effect of the primordial solar nebula. Icarus **191**(2), 413–433 (2007). https://doi.org/10.1016/j.icarus.2007.05.003

Brasser, R., Duncan, M.J., Levison, H.F.: Embedded star clusters and the formation of the Oort cloud. III. Evolution of the inner cloud during the Galactic phase. Icarus **196**(1), 274–284 (2008). https://doi.org/10.1016/j.icarus.2008.02.016

Breiter, S., Ratajczak, R.: Vectorial elements for the Galactic disc tide effects in commentary motion. MNRAS **364**(4), 1222–1228 (2005). https://doi.org/10.1111/j.1365-2966.2005.09658.x

Delsemme, A.H.: Galactic tides affect the Oort cloud: an observational confirmation. AAP **187**, 913–918 (1987)

Dones, L., Weissman, P.R., Levison, H.F., Duncan, M.J.: Oort cloud formation and dynamics, ed. by M.C. Festou, H.U. Keller, H.A. Weaver 2004, p. 153

Duncan, M., Quinn, T., Tremaine, S.: The formation and extent of the solar system comet cloud. AJ **94**, 1330–1338 (1987). https://doi.org/10.1086/114571

Dybczyński, P.A., Królikowska, M.: Where do long-period comets come from? Moving through the Jupiter–Saturn barrier. MNRAS **416**, 51–69 (2011). https://doi.org/10.1111/j.1365-2966.2011.19005.x

Emel'yanenko, V.V., Asher, D.J., Bailey, M.E.: The fundamental role of the Oort cloud in determining the flux of comets through the planetary system. MNRAS **381**, 779–789 (2007). https://doi.org/10.1111/j.1365-2966.2007.12269.x

Emel'yanenko, V.V., Asher, D.J., Bailey, M.E.: A model for the common origin of Jupiter family and Halley type comets. Earth Moon Planets **110**, 105–130 (2013). https://doi.org/10.1007/s11038-012-9413-z

Fernández, J.A.: The formation of the Oort cloud and the primitive Galactic environment. Icarus **129**(1), 106–119 (1997). https://doi.org/10.1006/icar.1997.5754

Fernández, J.A.: Evolution of comet orbits under the perturbing influence of the giant planets and nearby stars. Icarus **42**, 406–421 (1980). https://doi.org/10.1016/0019-1035(80)90104-9

Fernández, J.A.: New and evolved comets in the solar system. AAP **96**(1–2), 26–35 (1981)

Fernández, J.A., Ip, W.-H.: Dynamical evolution of a commentary swarm in the outer planetary region. Icarus **47**, 470–479 (1981). https://doi.org/10.1016/0019-1035(81)90195-0

Fernández, J.A., Brunini, A.: The buildup of a tightly bound comet cloud around an early Sun immersed in a dense Galactic environment: numerical experiments. Icarus **145**, 580–590 (2000). https://doi.org/10.1006/icar.2000.6348

Fouchard, M., Froeschlé, C., Rickman, H., Valsecchi, G.B.: The key role of massive stars in Oort cloud comet dynamics. Icarus **214**, 334–347 (2011). https://doi.org/10.1016/j.icarus.2011.04.012

Fouchard, M., Rickman, H., Froeschlé, C., Valsecchi, G.B.: Planetary perturbations for Oort cloud comets. I. Distributions and dynamics. Icarus **222**, 20–31 (2013). https://doi.org/10.1016/j.icarus.2012.10.027

Fouchard, M., Rickman, H., Froeschlé, C., Valsecchi, G.B.: On the present shape of the Oort cloud and the flux of; new; comets. Icarus **292**, 218–233 (2017). https://doi.org/10.1016/j.icarus.2017.01.013

Fouchard, M., Froeschlé, C., Breiter, S., Ratajczak, R., Valsecchi, G.B., Rickman, H.: Methods for the study of the dynamics of the Oort cloud Comets II: modelling the Galactic tide, ed. by D. Benest, C. Froeschle, E. Lega, vol. 729, p. 273 (2007). https://doi.org/10.1007/978-3-540-72984-6_10

Fouchard, M., Higuchi, A., Ito, T., Maquet, L.: The "memory" of the Oort cloud. AAP **620**, 45 (2018). https://doi.org/10.1051/0004-6361/201833435

Heisler, J., Tremaine, S.: The influence of the Galactic tidal field on the Oort comet cloud. Icarus **65**(1), 13–26 (1986). https://doi.org/10.1016/0019-1035(86)90060-6

Higuchi, A., Kokubo, E.: Effect of stellar encounters on comet cloud formation. AJ **150**, 26 (2015). https://doi.org/10.1088/0004-6256/150/1/26

Higuchi, A., Kokubo, E., Kinoshita, H., Mukai, T.: Orbital evolution of planetesimals due to the Galactic tide: formation of the comet cloud. AJ **134**, 1693–1706 (2007). https://doi.org/10.1086/521815

Hills, J.G.: Comet showers and the steady-state infall of comets from the Oort cloud. AJ **86**, 1730–1740 (1981). https://doi.org/10.1086/113058

Kaib, N.A., Quinn, T.: The formation of the Oort cloud in open cluster environments. Icarus **197**(1), 221–238 (2008). https://doi.org/10.1016/j.icarus.2008.03.020

Kaib, N.A., Quinn, T.: Reassessing the source of long-period comets. Science **325**, 1234 (2009). https://doi.org/10.1126/science.1172676

Leinert, C., Bowyer, S., Haikala, L.K., Hanner, M.S., Hauser, M.G., Levasseur-Regourd, A.-C., et al.: The 1997 reference of diffuse night sky brightness. AAPS **127**, 1–99 (1998). https://doi.org/10.1051/aas:1998105

Matese, J.J., Whitman, P.G.: A model of the Galactic tidal interaction with the Oort comet cloud. Celest. Mech. Dyn. Astron. **54**(1–3), 13–35 (1992). https://doi.org/10.1007/BF00049541

Nesvorný, D., Vokrouhlický, D., Dones, L., Levison, H.F., Kaib, N., Morbidelli, A.: Origin and evolution of short-period comets. APJ **845**, 27 (2017). https://doi.org/10.3847/1538-4357/aa7cf6

Nordlander, T., Rickman, H., Gustafsson, B.: The destruction of an Oort Cloud in a rich stellar cluster. AAP **603**, 112 (2017). https://doi.org/10.1051/0004-6361/201630342

Oort, J.H.: The structure of the cloud of comets surrounding the Solar System and a hypothesis concerning its origin. Bull. Astron. Inst. Neth. **11**, 91–110 (1950)

Öpik, E.: Note on stellar perturbations of nearby parabolic orbit. Proc. Am. Acad. Arts Sci. **67**, 1659–1683 (1932)

Rickman, H., Fouchard, M., Froeschlé, C., Valsecchi, G.B.: Injection of Oort Cloud comets: the fundamental role of stellar perturbations. Celest. Mech. Dyn. Astron. **102**, 111–132 (2008). https://doi.org/10.1007/s10569-008-9140-y

Tsiganis, K., Gomes, R., Morbidelli, A., Levison, H.F.: Origin of the orbital architecture of the giant planets of the Solar System. Nature **435**, 459–461 (2005). https://doi.org/10.1038/nature03539

Vokrouhlický, D., Nesvorný, D., Dones, L.: Origin and evolution of long-period comets. AJ **157**(5), 181 (2019). https://doi.org/10.3847/1538-3881/ab13aa

Whipple, F.L.: On the distribution of sernimajor axes among comet orbits. AJ **67**, 1–9 (1962). https://doi.org/10.1086/108596

Wiegert, P., Tremaine, S.: The evolution of long-period comets. Icarus **137**(1), 84–121 (1999). https://doi.org/10.1006/icar.1998.6040